Focusing of an Explosive Plasma Expansion in a Transverse Magnetic Field

C. Plechaty,* R. Presura,† and A. A. Esaulov‡

University of Nevada, Reno, Reno, Nevada 89557, USA

(Received 10 October 2011; revised manuscript received 31 July 2013; published 31 October 2013)

The dynamics of a laser ablation plasma expanding in an external magnetic field have been investigated with imaging interferometry and shadowgraphy. The diagnostics reveal a new interaction mechanism, namely, the redirection of the explosive plasma expansion into a converging flow. A comparison with three-dimensional ideal magnetohydrodynamic simulation results supports the observation that the efficient lateral plasma confinement causes the plasma to converge on the axis and initiate a directed flow. The resulting collimated flow propagates across the magnetic field in a kinetic regime, which cannot be modeled within the same framework.

DOI: 10.1103/PhysRevLett.111.185002 PACS numbers: 52.25.Xz, 52.30.−q

Plasma–magnetic-field interactions frequently govern the dynamics and the stability of laboratory and astrophysical systems. Controlled laboratory investigations of such interactions, conducted with laser ablation plasma expanding in an external magnetic field, have previously produced two types of outcomes. In the first case, directed plasma flows become polarized and cross the magnetic field due to $\mathbf{E} \times \mathbf{B}$ drift [1–4]. In the second case, plasma deceleration at the interface with the magnetic field leads to the growth of flute instabilities [5–11]. In these studies, the ion Larmor radius was comparable with or larger than the plasma scale length. In this kinetic regime, the instabilities observed were the unmagnetized ion Rayleigh-Taylor instability [12], also known as the large-Larmor-radius Rayleigh-Taylor instability, and the lower hybrid drift instability [13,14]. These instabilities grow as the flutes become polarized and expand directionally via $\mathbf{E} \times \mathbf{B}$ drift [7,15].

In the this Letter, a novel effect of a transverse magnetic field on the expansion of a laser-produced plasma is reported. The initial explosive, quasi-isotropic plasma expansion is redirected into a narrow directed flow. To our knowledge, this behavior has not been observed before in any experiments.

A schematic of the experimental setup employed is shown in Fig. 1. Plasma was produced by ablating a flat polyethylene target with a 1058 nm wavelength laser beam with 8 J of energy and a 0.5 ns duration (irradiance on a target of $\sim 5 \times 10^{14}\ \mathrm{W/cm^2}$). The plasma expanded in the external magnetic field generated by passing a 0.65 MA current with a 200 ns rise time through an electrode with a flat face parallel to the target surface. At maximum current, the strength of the magnetic field was numerically computed [16] to vary from 13 T at the electrode surface to about 7 T near the target surface. The distance between the target and electrode surfaces was 10 mm. To minimize the effect of the ambient gas, the chamber was evacuated to less than 10 μTorr, which is much lower than the plasma and magnetic field pressure in the interaction region.

Pulsed laser interferometry and shadow imaging were employed along the same line of sight (x, coordinates shown in Fig. 1) to analyze the interaction between the expanding plasma and the magnetic field. The plasma was imaged in the y-z plane, perpendicular to the magnetic field. Interferometry provided the sight-line–integrated plasma density distribution $n_l(y, z) \equiv \int n_e(x, y, z)dx$, where n_e is the electron number density. The plasma expansion velocity u was determined from the lowest measurable n_l. Shadowgraphy provided information about the plasma distribution via probing beam absorption (by inverse bremsstrahlung) and refraction (on plasma density gradients). The probing laser beam had an energy $E <$ 90 mJ (producing insignificant plasma heating) and a pulse duration of 0.2 ns (much shorter than the dynamic time scale). Its 1064 nm wavelength provided a minimum density resolution $n_{l,\min} \approx 5.6 \times 10^{17}\ \mathrm{cm^{-3}\,mm}$ (corresponding to 0.2 fringe shifts). The delay between the probing beam and the heating beam t was varied at each shot and was measured with a pair of photodiodes.

To assist in the understanding of the plasma dynamics in an external magnetic field, numerical modeling was performed with AW-MHD [17], a three-dimensional ideal MHD

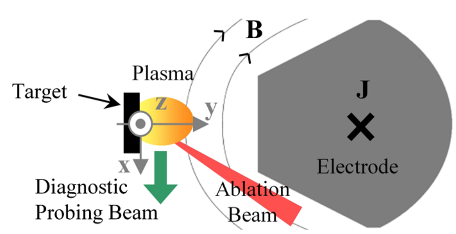

FIG. 1 (color online). Experimental setup. $\mathbf{J}$ is the current density vector and $\mathbf{B}$ is the magnetic field vector. Coordinate system: The y axis is perpendicular to the target surface and points toward the electrode along the magnetic field gradient, the z axis is antiparallel to $\mathbf{J}$, and the x axis is the laser probe propagation direction. The origin is located in the center of the focal spot on the target surface.

code. In simulations it was assumed that a portion E_{HS} of the laser energy was instantly and uniformly deposited in a cylindrically shaped region [hot spot (HS)] of the target of radius $r_{HS} = 50\ \mu m$ and depth d_{HS}. The best match of the simulation results with the experimental data was obtained for $E_{HS} = 1$ J and $d_{HS} = 2.5\ \mu m$.

In the absence of a magnetic field, the laser ablation plasma expands unimpeded in vacuum. Interferometry shows that n_l decreases monotonically with the distance from the target [Figs. 2(a) and 2(b)]. The only region with a noticeable electron density gradient forms near the laser spot, this being the main feature observed in shadowgrams [Figs. 2(c) and 2(d)]. It can be noted in interferograms that the plasma expansion is quasispheroidal, proceeding approximately two times faster in a direction normal to the target (y) than along the target surface (z).

When the plasma is generated in an external magnetic field, the expansion starts similarly to the $B = 0$ case, as seen by comparing Fig. 3(a) (obtained with $B \approx 10$ T) with Fig. 2(a) (recorded at the same time for $B = 0$). This similarity holds as long as the plasma pressure remains much larger than the field pressure in the interaction region.

As the laser plasma continues to expand in an external magnetic field, its pressure decreases and, for $t \gtrsim 6$ ns, it becomes comparable to the magnetic field pressure. This results in significant plasma deceleration. The expansion velocity anisotropy, as noted earlier when the magnetic field was absent, is also present when the field is applied and marks the plasma evolution. For $t \approx 6$–9 ns, the plasma expansion along y is decelerated with $g = 2 \pm 1 \times 10^{13}\ \mathrm{m/s^2}$. This leads to the formation of a second region of a noticeable density gradient at the plasma-field interface. Plasma continuing to expand from the target accumulates behind this decelerated region, leading to a local density

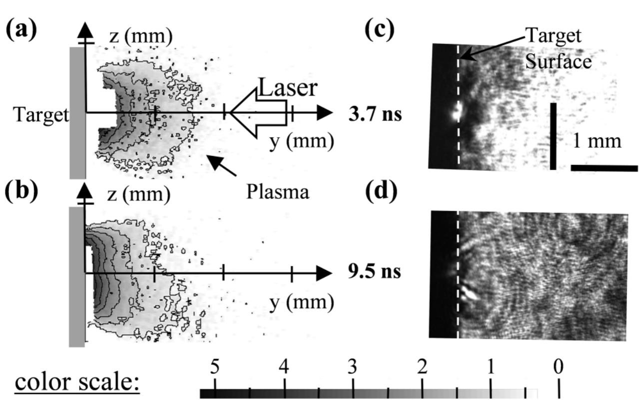

FIG. 2. Plasma expansion for $B = 0$, characterized by (a)–(b) linear plasma density n_l reconstructed from interferograms and (c)–(d) shadowgraphy. Images are taken for the following expansion times: (a) and (c) at $t \approx 3.7$ ns, (b) and (d) at $t \approx 9.5$ ns. Images (a) and (b) use the color scale shown (in units of $10^{18}\ \mathrm{cm^{-3}}$ mm) with isodensity contours drawn for clarity; in the white regions the fringe shift could not be determined due to insufficient n_l, refraction, or absorption of the probing beam.

increase, that progresses from the target in the y direction. This is illustrated in Fig. 3(b) by comparison with Fig. 2(b), which was obtained under the same conditions in the absence of the magnetic field. More importantly for the subsequent plasma dynamics, the magnetic field decelerates the plasma expansion in the z direction practically to stagnation. The corresponding density increases are evidenced by increased attenuation of the probe laser intensity in the shadowgram shown in Fig. 3(f), when compared with that in Fig. 2(d), obtained for $B = 0$. The density gradients are recorded in the shadowgram by the bright contours of the shadows [indicated by the arrow in Fig. 3(f)].

After $t \approx 10$ ns, in the presence of the magnetic field, the plasma flow is redirected to converge onto the y axis at $y \approx 3$ mm [Fig. 3(c)], an effect which to our knowledge has not been previously observed in laser–plasma–magnetic-field interactions. The plasma remains confined along z, as indicated by the shadowgram [Fig. 3(g)]. For $t \approx 10$–13 ns, the converging plasma evolves into a directed flow. After $t \gtrsim 19$ ns, the plasma expansion continues as a collimated flow along y [Fig. 3(d)], across the magnetic field, with a constant velocity $v_{pen} = 2.2 \pm 0.3 \times 10^5$ m/s.

The three-dimensional magnetohydrodynamic simulation results agree well with the experimental observations of the plasma expansion both with and without an external magnetic field, and provide parameters inaccessible experimentally to improve the understanding of the plasma evolution.

For the case of the zero magnetic field [Figs. 4(a) and 4(b)], the simulation performed reproduces well the experimentally measured time evolution of the plasma density distribution [Figs. 2(a) and 2(b), respectively]. It should be noted here that the MHD model does not tolerate vacuum. In order to bypass this difficulty, the vacuum region was prefilled with a background density, which at level $\rho_b = 5 \times 10^{-8}\ \mathrm{g/cm^3}$ was sufficiently low as to not noticeably affect the simulation results. The only deficiency of this approach is the generation of a weak and low-density shock wave, which is attached to the front of the expansion fan. However, the dynamics of the expansion fan itself adequately describes the process of plasma expansion into a vacuum for the plasma mass densities $\rho \gg \rho_b$.

For early times ($t \lesssim 4$ ns), when the plasma pressure is much larger than the field pressure, the simulations confirm the experimental observation that the expansion is similar when $B = 0$ [Fig. 4(a)] and when $B \neq 0$ [Fig. 4(c)]. One noticeable difference from the experiment [Fig. 3(a)] is a higher density halo around the plasma plume perimeter in the modeling [Fig. 4(c)], which is due to the deceleration of the low-density plasma expansion front by the magnetic field. If present, this structure would not be observed in experiments, because its density is lower than the detection limit of the interferometer.

Later during the expansion in the magnetic field, the simulations show the formation of high density gradients at the contact discontinuity separating the plasma from the

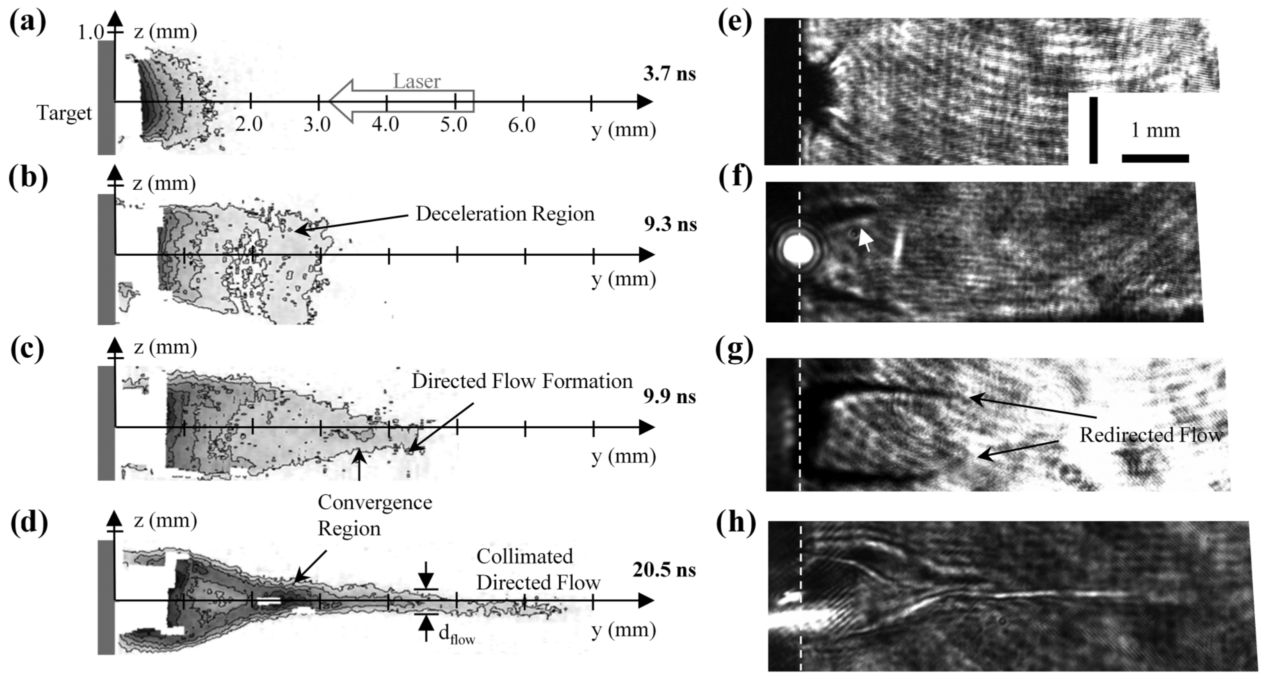

FIG. 3. Plasma expansion in an external magnetic field. (a)–(d) Line-integrated plasma density n_l, using the color scale of Fig. 2. (e)–(h) Shadowgrams recorded at the same time along the same line of sight as the corresponding interferograms. Each pair of images was obtained in a different shot. The magnetic field vector points into the page and its amplitude varies within less than 10% for the expansion times shown.

magnetic field [Figs. 4(d) and 4(g)]. On the other side of this discontinuity, strong gradients of the magnetic field induce surface currents that flow along the outer edge of the plasma flow. These surface currents effectively shield out the magnetic field from the expanding plasma jet. As shown in Fig. 4(f), the magnetic field magnitude rapidly drops to zero within the plasma forming a diamagnetic cavity and, thus, allowing plasma to expand freely in the y direction.

The lateral plasma confinement and the density accumulation behind the discontinuity observed in the experiment [Figs. 3(b)–3(d)] are also apparent in the simulation [Figs. 4(c)–4(e)], especially in the vicinity of the target. The overall shape of the discontinuity can be explained by examining the plasma flow, indicated by the vector field in Fig. 4(d). Because of the preferential expansion profile, the z velocity component of the interior plasma flow decreases as y increases, resulting in a corresponding decrease in the ram pressure. Additionally, as y increases so does the magnetic pressure since the magnetic field gradient is oriented along y. Thus, the distance along z at which the boundary forms is shorter when it is farther from the target. For later times ($t \gtrsim 10$ ns), the driving pressure of the plasma flow from the target decreases, and the volume enclosed by the plasma-field boundary decreases too. This effect, observed in the experiment [by comparing Fig. 3(d) with Fig. 3(c)], is well reproduced by simulations [Figs. 4(e) and 4(d)].

Around $t \approx 9$–10 ns, the plasma flow converges onto the y axis at $y \approx 3$ mm [Figs. 3(c) and 3(d)]. The velocity orientation maps obtained from the AW-MHD simulations (Fig. 4) are indicative of the mechanism responsible for the formation of this converging flow. As plasma continues to expand from the target region into which laser energy was deposited, its flow is redirected by the higher density plasma accumulated along the discontinuity. Because of the shape of the boundary, the plasma is eventually guided toward the axis forming a region of converging flow [Fig. 4(d)], labeled as the "convergence region" in Figs. 3(c) and 3(d). The driving mechanism for this behavior is similar to that suggested in Ref. [18], which considered a spherical stellar wind expanding into ambient gas with a one-dimensional pressure gradient. In our experiment the magnetic field plays the role of the ambient gas, redirecting the plasma flow and producing the converging flow. To our knowledge, this mechanism has not been observed to date in laboratory experiments of this kind. At the convergence region the pressure increases, leading to plasma ejection in the direction of the pressure gradient, y [Fig. 3(c)], as described in Ref. [19].

The final aspect of the plasma's evolution left out of the preceding discussion is the propagation of the collimated flow across the magnetic field [Figs. 3(d) and 3(h)]. The ideal MHD description employed above to describe the plasma dynamics is adequate for explaining the redirection of the explosive plasma flow into a converging flow and the initiation of a directed flow. However, the propagation of this collimated flow across the magnetic field is not well captured by this model. Later in time ($t \gtrsim 10$ ns), farther from the target along its normal ($y \gtrsim 2.5$ mm), the simulation results show additional details not observed in the experiment,

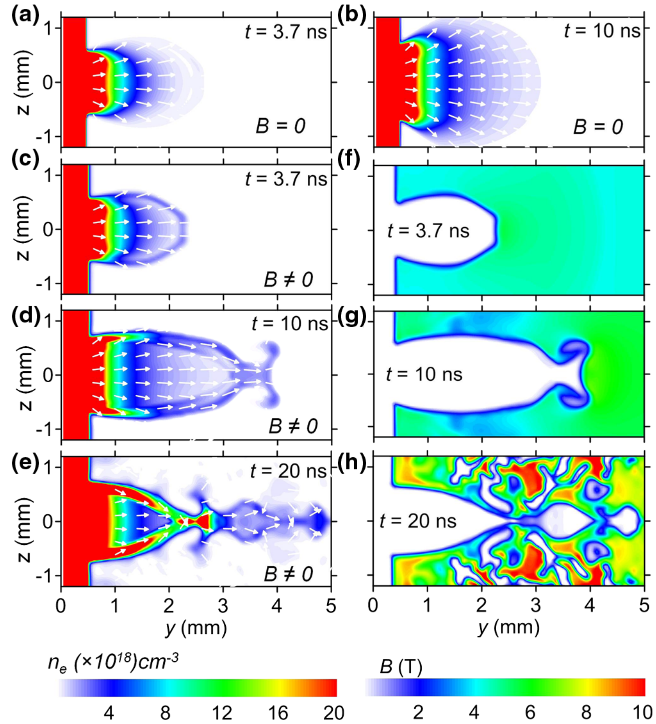

FIG. 4 (color online). AW-MHD results for n_e in the y-z plane for (a)–(b) $B = 0$ and (c)–(e) $B \neq 0$. In panels (a)–(e), arrows denote the direction of the plasma velocity vector in the plane of the image. (f)–(h) AW-MHD results for the magnitude of the magnetic field in the same plane.

as indicated by comparing Figs. 4(d) and 4(e) with Figs. 3(c) and 3(d), respectively. The origin of this discrepancy can be understood by examining the plasma conditions in the collimated flow region [Fig. 3(d)]. For the values of n_e observed in this region, the fact that the probe laser beam is not significantly attenuated by inverse bremsstrahlung absorption [20] indicates $T_e \geq 10$ eV, for which the average ion charge state $Z > 2$. An upper bound for $T_e \leq 200$ eV, is determined from taking the maximum value obtained for early times in simulation. For $d_{\text{flow}} \approx 0.3$ mm, determined from refractometric imaging [Fig. 3(d)], the lateral field resistively diffuses into the collimated flow plasma on a $\sim$1 ns time scale. However, the plasma interaction with the magnetic field is not simply a diffusive process. To illustrate this, from interferometry [Fig. 3(d)] $n_l \approx n_e l_x = 10^{18}$ cm^{-3} mm (l_x is the plasma extent along the probing direction x), and the magnetic field strength at the front is $B \approx 10$ T. For these parameters, the Hall coefficient $H \equiv c v_A / L_z \omega_{pi} u$ [4] (where c/ω_{pi} is the ion skin depth, v_A is the Alfvén velocity, and $L_z \approx 0.15$ mm and characterizes the density gradient scale length) has values $H \sim 1.7$ (within a factor of 2 to account for uncertainty in l_x). Therefore, the Hall effect is significant within the collimated flow, and allows for a more rapid magnetic field penetration into the plasma [21] than resistive diffusion alone. Indeed, the Hall penetration velocity can be estimated in the context of Hall MHD [22] as $v_H = B/2\mu_0 n_e e L_z$. For our parameters, $v_H \approx 1.7 \pm 0.9 \times 10^5$ m/s, similar to the experimentally measured value of $v_{\text{pen}} = 2.2 \pm 0.3 \times 10^5$ m/s.

The plasma parameters indicate that magnetic field diffusion plays an important role in the plume evolution into a narrow, collimated flow. This behavior can be understood noting that as the diffusion occurs, a self-polarization field [2,23–25] $\mathbf{E}_p = -E\hat{\mathbf{z}}$, is established across the plasma. The plasma polarization results from the accumulation of charge along the $\pm z$ boundaries, and is upheld as long as the plasma dielectric constant $\epsilon \approx 1 + (\omega_{pi}/\omega_{ci})^2$ is large (ω_{pi} is the plasma frequency and ω_{ci} is the ion cyclotron frequency). For the plasma parameter values in this region, $\epsilon \sim 10^6$. The plasma simultaneously magnetized in the x direction and polarized along z then crosses the field by $\mathbf{E}_p \times \mathbf{B}$ drift. This explanation is supported by the observation that the collimated flow deviates from the y direction [Figs. 3(c)–3(h)], which is due to polarization at the flow front [2].

In summary, a previously unexplored type of interaction between a laser-produced plasma flow and a magnetic field was identified and investigated. A plasma plume preferentially expanding along the target normal in the absence of a magnetic field is confined laterally and turns into a directed plasma flow when a field is applied. The lateral confinement leads to a redirection of the interior plasma originating from the target region heated by the ablation laser. The redirection mechanism is similar to that proposed in Ref. [18], with the difference that in our experiment the magnetic field provides the external pressure profile required for the guidance of the explosive plasma flow. This pressure redirects the flow toward the axis, and this convergence generates a directed flow [19]. Diffusion of the magnetic field into the directed flow allows the flow to self-polarize with a field $\mathbf{E}_p$. The flow then penetrates the magnetic field due to $\mathbf{E}_p \times \mathbf{B}$ drift.

The authors would like to thank Dr. Sandra Stein, Leela O'Brien, Showera Haque, and Matthew Tooth for their help during the experiment, and Dr. Gennady Sarkisov for designing the interferometry and shadow diagnostics. This work was performed at the Nevada Terawatt Facility and supported by the U.S. DOE under Cooperative Agreement No. DE-FC52-06NA27616.

*Present address: Lawrence Livermore National Laboratory, 7000 East Avenue, Livermore, California 94550, USA.
plechaty5@llnl.gov
†presura@unr.edu
‡esaulov@unr.edu

[1] J. Bruneteau, E. Fabre, H. Lamain, and P. Vasseur, Phys. Fluids **13**, 1795 (1970).
[2] A. N. Mostovych, B. H. Ripin, and J. A. Stamper, Phys. Rev. Lett. **62**, 2837 (1989).

[3] T. Peyser, C. Manka, B. Ripin, and G. Ganguli, Phys. Fluids B **4**, 2448 (1992).
[4] C. Plechaty, R. Presura, S. Stein, D. Martinez, S. Neff, V. Ivanov, and Y. Stepanenko, High Energy Density Phys. **6**, 258 (2010).
[5] S. Okada, K. Sato, and T. Sekiguchi, Jpn. J. Appl. Phys. **20**, 157 (1981).
[6] G. Dimonte and L. Wiley, Phys. Rev. Lett. **67**, 1755 (1991).
[7] B. Ripin, J. Huba, E. McLean, C. Manka, T. Peyser, H. Burris, and J. Grun, Phys. Fluids B **5**, 3491 (1993).
[8] A. Kasperczuk, T. Pisarczyk, and Y. Zakharov, Laser Part. Beams **17**, 537 (1999).
[9] R. Presura *et al.*, Astrophys. Space Sci. **298**, 299 (2005).
[10] Yu. P. Zakharov, V. M. Antonov, E. L. Boyarintsev, A. V. Melekhov, V. G. Posukh, I. F. Shaikhislamov, and V. V. Pickalov, Plasma Phys. Rep. **32**, 183 (2006).
[11] C. Plechaty, R. Presura, S. Wright, S. Neff, and A. Haboub, Astrophys. Space Sci. **322**, 195 (2009).
[12] A. Hassam and J. Huba, Phys. Fluids **31**, 318 (1988).
[13] N. Krall and P. Liewer, Phys. Rev. A **4**, 2094 (1971).
[14] R. Davidson, N. Gladd, C. Wu, and J. Huba, Phys. Fluids **20**, 301 (1977).
[15] J. Huba and S. Ossakow, J. Atmos. Terr. Phys. **43**, 775 (1981).
[16] C. Plechaty, Ph.D. thesis, University of Nevada, Reno, 2011.
[17] A. A. Esaulov, V. L. Kantsyrev, A. S. Safronova, A. L. Velikovich, M. E. Cuneo, B. Jones, K. W. Struve, and T. A. Mehlhorn, Phys. Plasmas **15**, 052703 (2008).
[18] A. Frank, B. Balick, and M. Livio, Astrophys. J. **471**, L53 (1996).
[19] J. Canto, G. Tenorio-Tagle, and M. Rozyczka, Astron. Astrophys. **192**, 287 (1988).
[20] T. Johnston and J. Dawson, Phys. Fluids **16**, 722 (1973).
[21] J. Huba, Phys. Plasmas **2**, 2504 (1995).
[22] A. S. Kingsep, Yu. V. Mohkov, and K. V. Chukbar, Sov. J. Plasma Phys. **10**, 495 (1984).
[23] J. Lemaire, J. Plasma Phys. **33**, 425 (1985).
[24] G. Schmidt, Phys. Fluids **3**, 961 (1960).
[25] N. Brenning, T. Hurtig, and M. Raadu, Phys. Plasmas **12**, 012309 (2005).